Progress of Theoretical Physics, Vol. 83, No. 3, March 1990

Gravitational Lens Effect on the Images of High Redshift Objects

Kenji TOMITA and Kazuya WATANABE

Research Institute for Theoretical Physics
Hiroshima University, Takehara, Hiroshima 725

(Received December 14, 1989)

Solving numerically the null geodesic equations in an inhomogeneous model universe consisting of galaxies, we study the gravitational lens effect of galaxies on the images of high redshift objects. Morphological studies are done as well as quantitative analyses for the image deformation. For the spatial distribution of galaxies, it is assumed that the present correlation length is about $5h^{-1}$ Mpc (the Hubble constant $H_0=100h$ kms^{-1}Mpc^{-1}). It is shown that the images of the objects with $z\geq 2$ can be much deformed in angular sizes of several arcsec. This result shows that the warped structure of radio images in high redshift quasars may be explained by the gravitational lens effect.

§ 1. Introduction

The light rays emitted by high redshift objects like quasars propagate through the intergalactic space, the neighbourhood and sometimes the inside of galaxies before they reach us. Their paths are more or less deflected by the gravitational forces of galaxies. In the recent observational studies on the morphologies of high redshift quasars, many interesting distorted or warping images were found.[1),2)] It seems to us that they originate in gravitational lensing by galaxies. In this paper we study what deformation is aroused by the galactic lens effect on the images of high redshift objects. The image deformation was once investigated by Blandford and Jaroszynski,[3)] who took into account the inhomogeneous distribution of lenses by using the two-point correlation function. In the present treatment we consider also the inhomogeneity of mass distribution in individual galaxies as well as their spatial distribution. Both of these two inhomogeneities are important factors for image deformation.

The deflection angles depend on the galactic masses and radii, the number density, the birth time of galaxies and the background cosmological model. If we take into account the dark matter in the galactic halo region, the galactic masses are by a factor 10—100 larger than the standard mass ($\sim 10^{11}$ M$_\odot$). In this paper we adopt the rather large value for the galactic mass and the Einstein-de Sitter background model. For the galactic distribution we assume that the present correlation length is about $5h^{-1}$ Mpc (the Hubble constant $H_0=100h$ kms^{-1}Mpc^{-1}), but for a comparison the case when all galaxies are put always at the grid points is also discussed.

In § 2 we explain briefly the method in which our inhomogeneous model universe is derived and the null geodesic equations are solved. In § 3 we treat the propagation of ten ray bundles in the ten different directions. Each bundle consists of 900 rays. By analyzing the deflection of the ray bundles the image deformation is morphologically studied in various cases. In § 4 two quantities representing the image deformation are defined and they are quantitatively analyzed. In § 5 it is shown that

some characteristic behaviors of deformation can be derived in a simplified model of multiple deflections. In § 6 concluding remarks are given. In Appendix our numerical methods are shown.

§ 2. Equations of light propagation in inhomogeneous models

The background model is assumed to be spatially flat and, in the Newtonian approximation, the line-element of inhomogeneous models is expressed as

$$ds^2=-(1+2\varphi/c^2)c^2dt^2+(1-2\varphi/c^2)a(t)^2d\boldsymbol{x}^2\,, \tag{2·1}$$

where $a(t)=(t/t_1)^{2/3}$ and t_1 denotes an initial time. The gravitational potential φ satisfies

$$a^{-2}\frac{\partial^2\varphi}{\partial\boldsymbol{x}^2}=4\pi G(\rho(\boldsymbol{x})-\rho_B)\,, \tag{2·2}$$

where ρ_B is the background density satisfying $6\pi G\rho_B t^2=1$. In our treatment the inhomogeneities are spatially periodic in the sense that the physical situation at $\boldsymbol{x}$ is the same as that at $\boldsymbol{x}+l_1\boldsymbol{n}$, where $\boldsymbol{n}(=(n^1, n^2, n^3))$ are integers. In an arbitrary box with coordinate volume $V_1(\equiv l_1^3)$ there are N particles representing galaxies with the same mass m. It is assumed that the force at an arbitrary point is the sum of forces from N particles in the box whose center is its relevant point, and that the forces from outside the box can be neglected. This calculation method was used in Miyoshi and Kihara's work[4] and our previous paper.[5] If the size of the box is smaller than the characteristic size of inhomogeneities, this method is not good.

In our model the present length of a box is $(1+z_1)V_1^{1/3}=33.3h^{-1}$Mpc and the particle number N is 11^3, so that the mass is

$$m=\frac{3}{8\pi G}H_0^2V_1(1+z_1)^3/N=7.9\times10^{12}h^{-1}\mathrm{M}_\odot\,, \tag{2·3}$$

where z_1 is the redshift at an initial epoch t_1 and is taken as $1+z_1=100$ in the following. It is assumed that the particles are formed at epoch t_f such as $1+z_f\geq2$ and their physical radii are constant from the formation time to the present. The above mass is the one which includes the mass of halo gas existing outside the optically seen region.

The matter density distribution in a particle is introduced by means of softening of the Newtonian forces, as in the previous paper,[5] and the effective radius l_{eff} is here taken to be 60, 80 or $120h^{-1}$kpc (see Appendix). This radius is rather larger than the standard galactic radius because the extended halo region is considered.

The light propagation is described by use of the ray vector

$$k^\mu=\frac{dx^\mu}{dv} \tag{2·4}$$

satisfying the null condition

$$k^\mu k_\mu=0 \tag{2·5}$$

and the null geodesic equations

$$k^{\mu}{}_{;\nu}k^{\nu}=0\,. \tag{2·6}$$

Now let us introduce the dimensionless time τ and spatial coordinates $y^i(i=1, 2, 3)$ defined by

$$\tau\equiv\frac{1}{3}\ln\left(\frac{t}{t_1}\right), \qquad y^i\equiv x^i/R\,, \tag{2·7}$$

where

$$R\equiv(V_1/N)^{1/3} \tag{2·8}$$

and the range of y^i is $[-L, L]$ with $L\equiv 0.5N^{1/3}$. Then the line-element is rewritten as

$$ds^2=-(3ct_1)^2e^{6\tau}(1+\alpha\phi)d\tau^2+R^2e^{4\tau}(1-\alpha\phi)d\boldsymbol{y}^2\,, \tag{2·9}$$

where

$$\alpha\equiv\frac{2Gm}{c^2R}=2.4\times10^{-7} \qquad \text{and} \qquad \varphi\equiv\frac{Gm}{R}\phi\,. \tag{2·10}$$

Moreover let us define K^i and $\tilde{K}^i$ by

$$K^{\mu}\equiv(K^0, K^i)=\frac{dy^{\mu}}{dv}\,, \tag{2·11}$$

$$\tilde{K}^i\equiv {c_R}^{-1}e^{-\tau}\frac{K^i}{K^0}\,, \tag{2·12}$$

where $y^0=\tau$ and c_R is the dimensionless light velocity defined by

$$c_R\equiv\frac{3ct_1}{R}=180\,, \tag{2·13}$$

and $K^i=K_i$. Then the equations for light paths are reduced to

$$\frac{dy^i}{d\tau}=c_Re^{\tau}\tilde{K}^i\,, \tag{2·14}$$

$$\frac{d\tilde{K}^i}{d\tau}=-\gamma{c_R}^{-1}e^{\tau}\left[\frac{\partial\phi_1}{\partial y^i}-2\frac{\partial\phi_1}{\partial y^j}\tilde{K}^j\tilde{K}^i\right]+\alpha\frac{\partial\phi}{\partial\tau}\tilde{K}^i\,, \tag{2·15}$$

$$\tilde{K}^i\tilde{K}_i=1+2\alpha\phi\,, \tag{2·16}$$

where

$$\gamma\equiv\alpha{c_R}^2=7.9\times10^{-3} \tag{2·17}$$

and the definition of ϕ_1 can be seen in Appendix. In the background model, $\tilde{K}^i$ is a constant unit vector ($\equiv\tilde{K}_B{}^i$) and light paths are given by

$$y_B{}^i=c_R(e^{\tau_0}-e^{\tau})\tilde{K}_B{}^i\,, \tag{2·18}$$

where τ_0 denotes the present epoch. If we consider the propagation from an epoch τ_f to the present epoch, we obtain

$$(y^i\tilde{K}_i)_B=c_R(1+z_1)^{1/2}\left[1-\frac{1}{(1+z_f)^{1/2}}\right], \tag{2·19}$$

where $\tau_1=0$, $e^{2\tau_0}=1+z_1$ and $e^{2\tau_f}=(1+z_1)/(1+z_f)$. The deflections of light paths in inhomogeneous models from the background paths at arbitrary epochs are defined as

$$\delta y^i\equiv y^i-y_B{}^i\,,\qquad \delta\tilde{K}^i\equiv\tilde{K}^i-\tilde{K}_B{}^i\,. \tag{2·20}$$

The parallel and vertical components of the deflections are given by

$$\delta_{\parallel}y^i=\delta y^j\tilde{K}_{Bj}\tilde{K}_B{}^i\,,\quad \delta_{\perp}y^i=\delta y^i-(\delta y^j\tilde{K}_{Bj})\tilde{K}_B{}^i\,. \tag{2·21}$$

In inhomogeneous models Eqs. (2·14) and (2·15) are solved in the past direction from the present epoch τ_0 to a past epoch τ_f. We set up the initial condition for rays as follows: First we consider the rays reaching the observer with $(y_B{}^i)_0$, i.e.,

$$(y^i)_0=(y_B{}^i)_0\qquad \text{for all rays}\,. \tag{2·22}$$

These rays are shot in the directions of $(\tilde{K}^i)_0$ which satisfy Eq. (2·16), and compared with corresponding rays with $(\tilde{K}_B{}^i)_0$ such as $(\tilde{K}^i)_0\propto(\tilde{K}_B{}^i)_0$. For $\tau\ll\tau_f$ the evolution of inhomogeneities is linear and the lens effect is comparatively small. It is not possible to take into account the evolution of particles at the stage $\tau\leq\tau_f$. Accordingly we give z_f as a parameter for simplicity and assume that at $\tau<\tau_f$ (or $z>z_f$) light streams freely through the background space. Here we take four values $z_f=1$, 2, 3 and 5.

For $\tau<\tau_f$ we get

$$\frac{dy^i}{d\tau}=c_Re^{\tau}(\tilde{K}^i)_f \tag{2·23}$$

or

$$y^i=(y^i)_f+c_R(\tilde{K}^i)_f(e^{\tau}-e^{\tau_f})\,, \tag{2·24}$$

where $(y^i)_f$ and $(\tilde{K}^i)_f$ mean y^i and $\tilde{K}^i$ at epoch τ_f.

§ 3. Morphology of image deformation

Now we consider an observer who is at the origin of a periodic box and receives the ray bundles incoming from many arbitrary directions. As shown in Fig. 1, each bundle consists of 900 rays which are put in the same separation angle (=1 arcsec) in a square region of 30 arcsec×30 arcsec at the present epoch. If we go back in time, the cross sections of ray bundles are deformed from the square to complicated forms.

In order to express angular positions of rays, we introduce two orthonormal vectors $e^i_{(1)}$ and $e^i_{(2)}$ in the plane perpendicular to the first ray vector, which satisfy the relations

$$e_{(1)}{}^ie_{(1)i}=e_{(2)}{}^ie_{(2)i}=1\,,\qquad e_{(1)}{}^ie_{(2)i}=0\,,\qquad e_{(1)}{}^i\tilde{K}_{Bi}=e_{(2)}{}^i\tilde{K}_{Bi}=0\,. \tag{3·1}$$

Even if for the above plane we take the planes perpendicular to any other rays, the difference which will appear in the following analyses is very small. Then the angular coordinates (X_α, Y_α) of 900 rays ($\alpha=1-900$) relative to the first ray ($\alpha=1$) are

defined by

$$X_\alpha \equiv [(\tilde{y}^i e_{(1)i})_\alpha - (\tilde{y}^i e_{(1)i})_1]/(y_B)_1 + X_1 ,$$
$$Y_\alpha \equiv [(\tilde{y}^i e_{(2)i})_\alpha - (\tilde{y}^i e_{(2)i})_1]/(y_B)_1 + Y_1 , \tag{3·2}$$

where

$$\tilde{y}^i \equiv y_B{}^i + \delta y^i \quad \text{and} \quad y_B{}^2 \equiv y_B{}^i y_{Bi} , \tag{3·3}$$

and (X_1, Y_1) is taken to be $(1, 1)$ in the arcsec unit. So far we have calculated light paths in ten ray bundles. The bundles are denoted as A, B, $\cdots$ and J. The cross section of a bundle is expressed for instance as $A_{80.2.3}$. This means the bundle index $=A$, $l_{\rm eff}=80h^{-1}$kpc, $z_f=2$ and $z_e=3$, where z_e denotes the redshift at the emission time. In Fig. 2 we show the examples of our calculations in the first ray bundle (A) for z_f and $z_e=1$, 2, 3 and 5 and the radius $l_{\rm eff}=80h^{-1}$kpc, that is, is, $A_{80.1.1}$, $A_{80.1.2}$, $A_{80.1.3}$, $A_{80.1.5}$, $A_{80.2.2}$, $A_{80.2.3}$, $A_{80.2.5}$, $A_{80.3.3}$, $A_{80.3.5}$ and $A_{80.5.5}$. Here $A_{80.2.1}$, $A_{80.3.1}$ and $A_{80.5.1}$ are equal to $A_{80.1.1}$, and $A_{80.3.2}$ and $A_{80.5.2}$ are equal to $A_{80.2.2}$. In Fig. 3 we show $B_{80.2.2}$, $C_{80.2.2}$, $\cdots$, $J_{80.2.2}$ to see the dependence on directions. In Fig. 4 we show $A_{60.2.2}$, $B_{60.2.2}$, $C_{60.2.2}$, $D_{60.2.2}$, $A_{120.2.2}$, $B_{120.2.2}$, $C_{120.2.2}$, and $D_{120.2.2}$ to see the dependence on the particle size.

From Fig. 2 we find that there is some morphological difference in the deformation of ray bundles in the following two cases:

Case 1($z_f=1$). Rays stream freely at $z\geq 1$,

Case 2($z_f\geq 2$). Rays stream freely at $z\geq 2$.

This means that galaxies at epoch $z\leq 2$ play dominant roles in the lens effect on high redshift objects. This trend is quantitatively analyzed in the next section and the explanation in a simplified model is given in § 5. Moreover it is found from Figs. 2 ~4 that often ray bundles focus and have caustic points or planes at epochs $z\sim 1$ and reexpand thereafter.

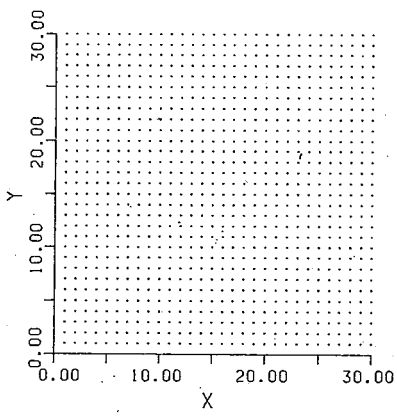

Fig. 1. Angular coordinates of rays in the ray bundle at the present epoch. The horizontal and vertical axes give the coordinates X and Y, respectively.

Next, we derive the deformed images which are brought by the lens effect to originally circular objects (with various layers) put at epochs $z_e=1-5$. Figure 5 shows the undeformed circular object. For this purpose we use the correspondence between the present and past positions of rays. Figure 6 shows deformed images in $A_{80.1.z}$, $A_{80.2.z}$, $A_{80.3.z}$ and $A_{80.5.z}$ for $z=1-5$, where the circular objects are put in the central region of the cross sections such as in Fig. 2. Figure 7 shows the images in $B_{80.2.z}$, $C_{80.2.z}$, $\cdots$, $J_{80.2.z}$ similarly. The layers are distinguished with the different symbols: $*$, $\times$, $\square$, and $|$ denote the regions

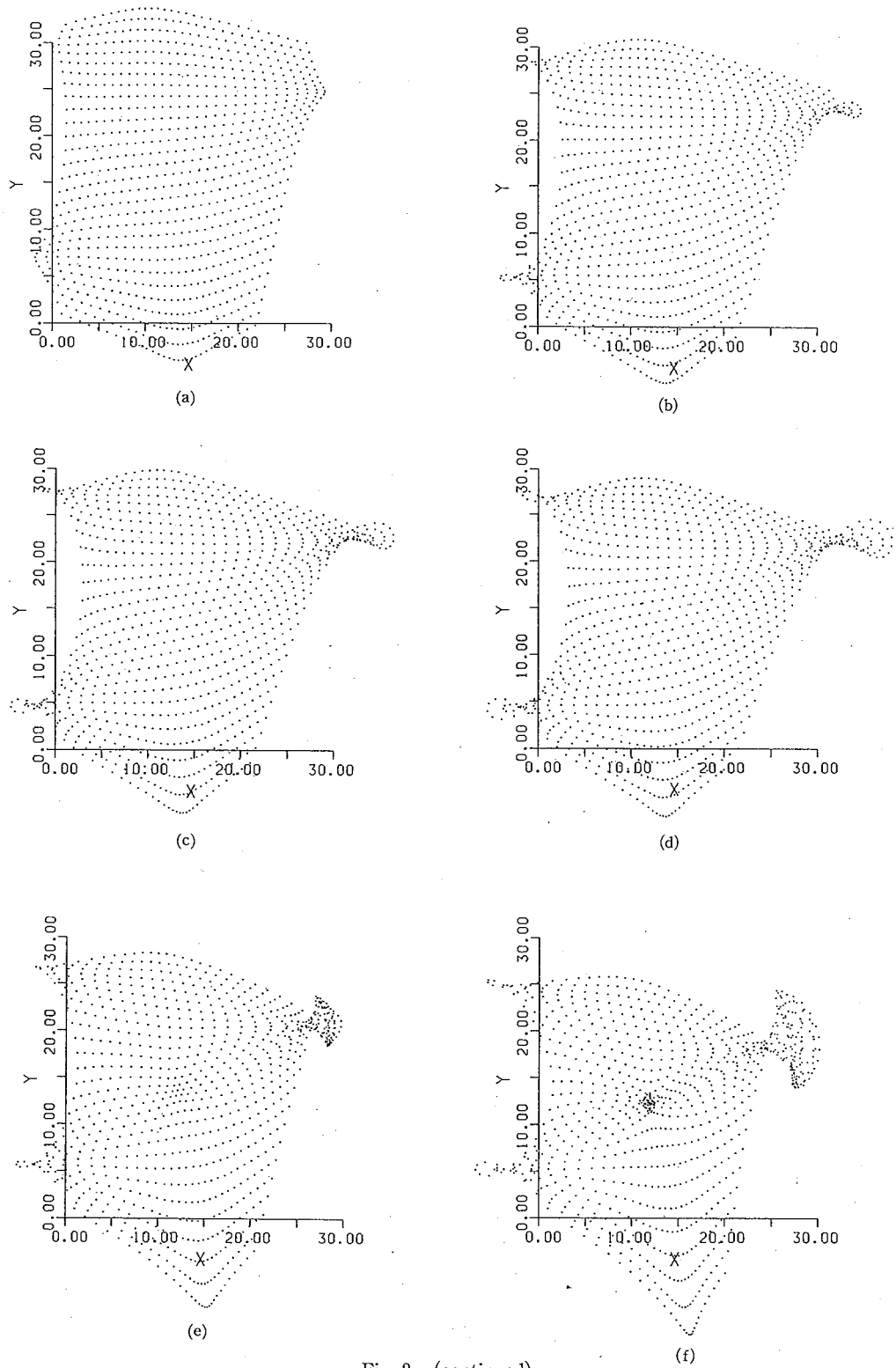

Fig. 2. (continued)

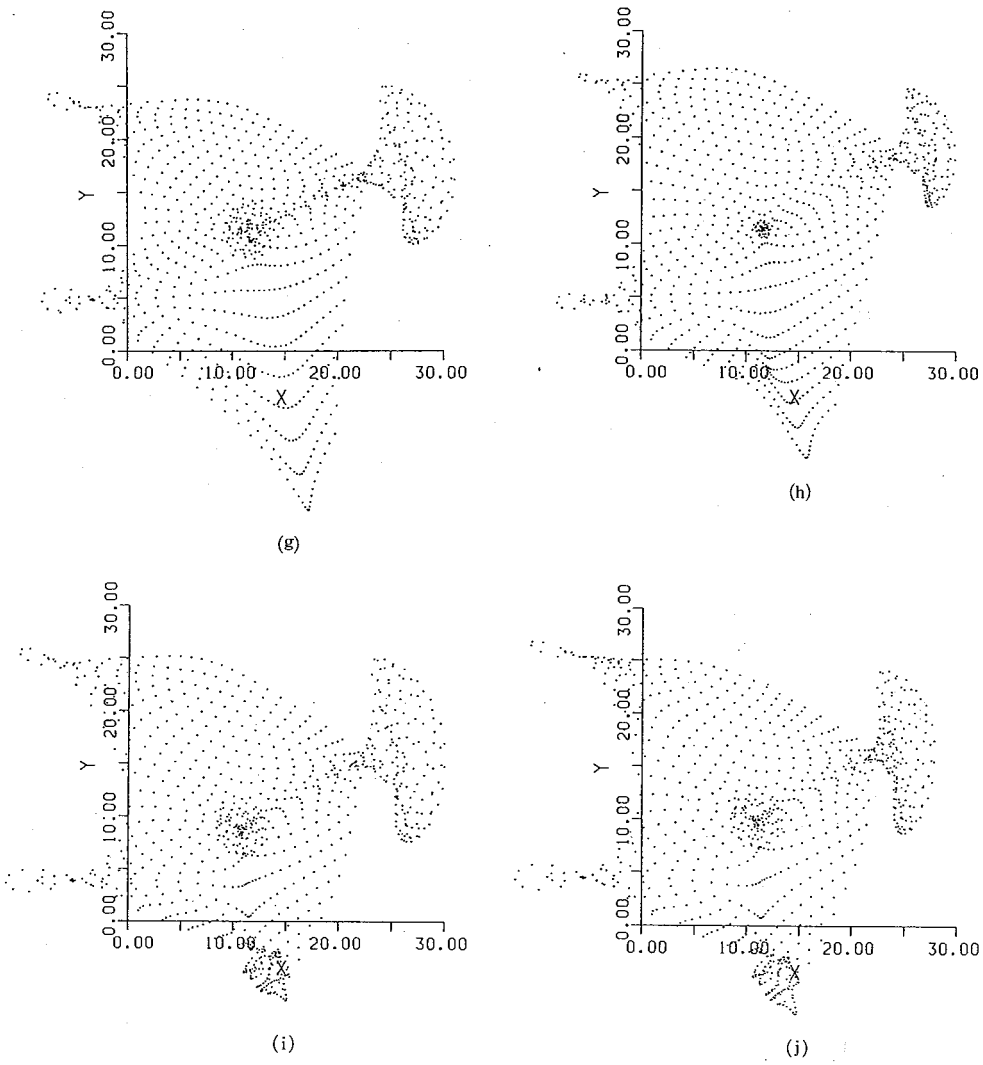

Fig. 2. Angular coordinates of rays in (a) $A_{80.1.1}$, (b) $A_{80.1.2}$, (c) $A_{80.1.3}$, (d) $A_{80.1.5}$, (e) $A_{80.2.2}$, (f) $A_{80.2.3}$, (g) $A_{80.2.5}$, (h) $A_{80.3.3}$, (i) $A_{80.3.5}$ and (j) $A_{80.5.5}$.

of $r \leq 1$, $1 < r \leq 2$, $2 < r \leq 3$ and $3 < r \leq 5$, respectively, where $r \equiv |\boldsymbol{r} - \boldsymbol{r}_c|$, $\boldsymbol{r} \equiv (X, Y)$ and $\boldsymbol{r}_c$ denotes the center. From the images in the ten ray bundles we find as general properties that the circular images are deformed to long and narrow shapes in most cases, and that for $r \leq 5$ the deformation in various layers is comparable.

Moreover let us consider linear objects with various parts put at epochs $z_e = 1-5$. Figure 8 shows the undeformed linear object. Then Fig. 9 shows how the lens effect warps the optical images of these objects in $A_{80.2.z}$, $B_{80.2.z}$ ⋯, $J_{80.2.z}$. These morphological changes are interesting when we compare them with the warping structure of high redsift quasars.[1),2)]

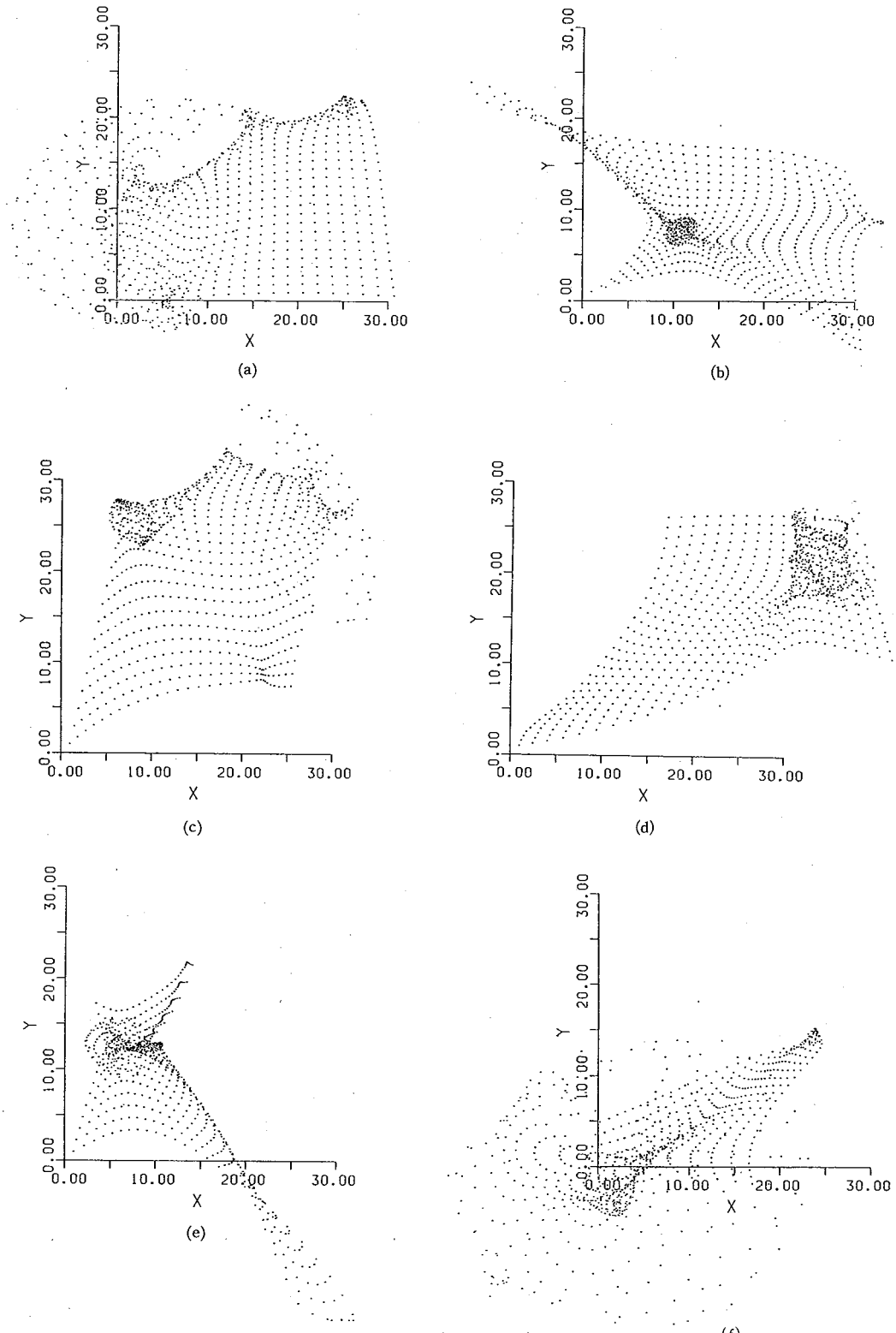

Fig. 3. (continued)

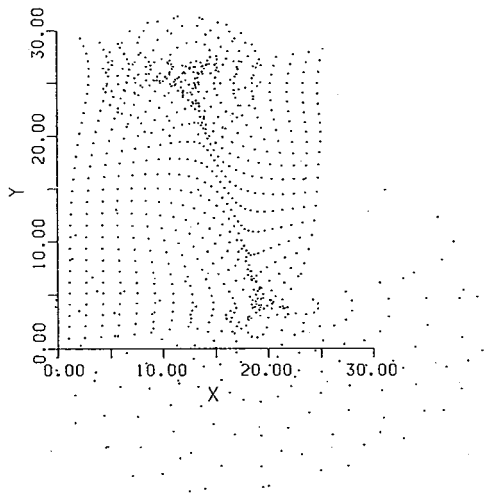

(g)

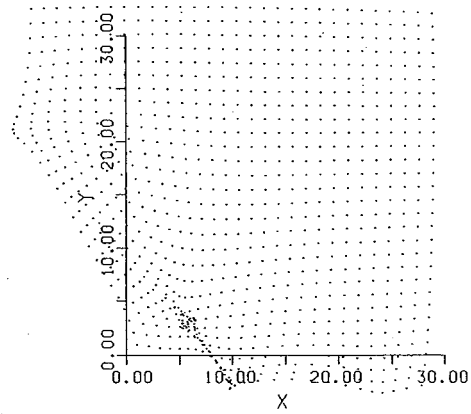

(h)

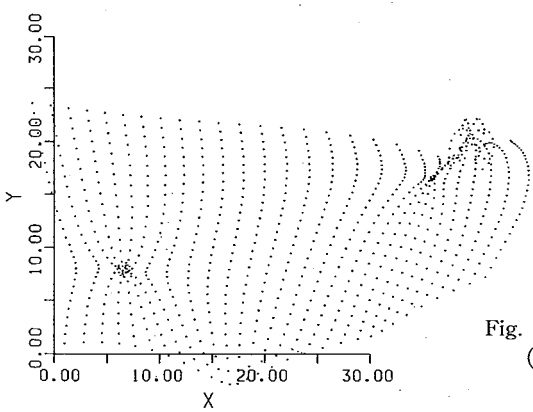

(i)

Fig. 3. Angular coordinates of rays in (a) $B_{80.2.2}$, (b) $C_{80.2.2}$, ···, (i) $J_{80.2.2}$.

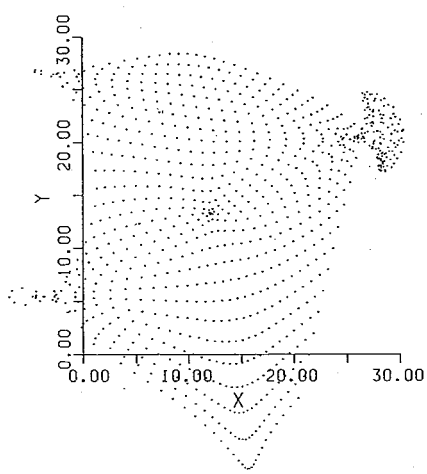

(a)

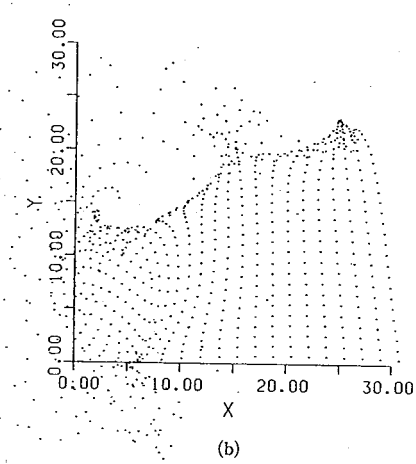

(b)

Fig. 4. (continued)

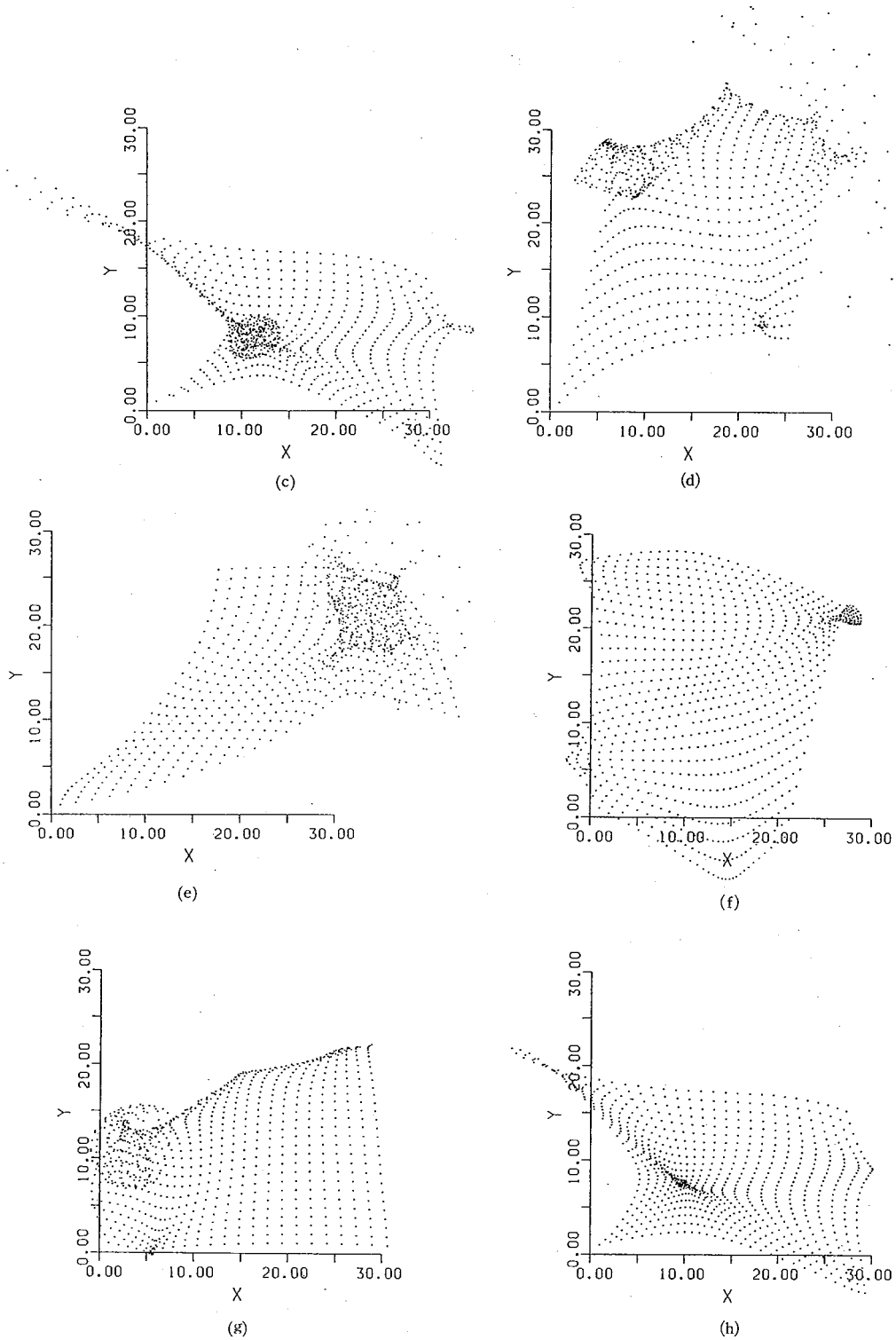

Fig. 4. (continued)

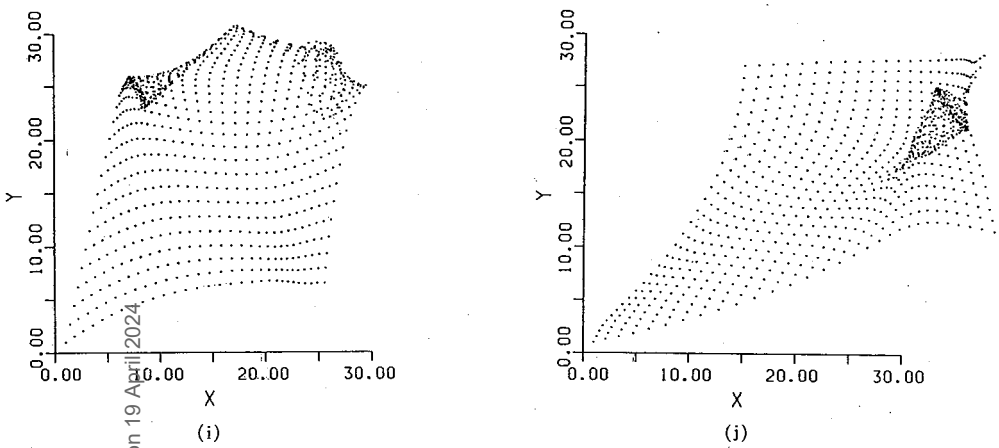

Fig. 4. Angular coordinates of rays in (a) $A_{60.2.2}$, (b) $B_{60.2.2}$, ···, (e) $E_{60.2.2}$, (f) $A_{120.2.2}$, (g) $B_{120.2.2}$, ···, (j) $E_{120.2.2}$.

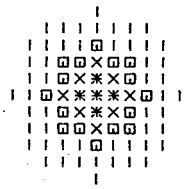

Fig. 5. Circular regions. ∗, ×, □, | denote the regions of $r \leq 1$, $1 < r \leq 2$, $2 < r \leq 3$ and $3 < r \leq 5$, respectively.

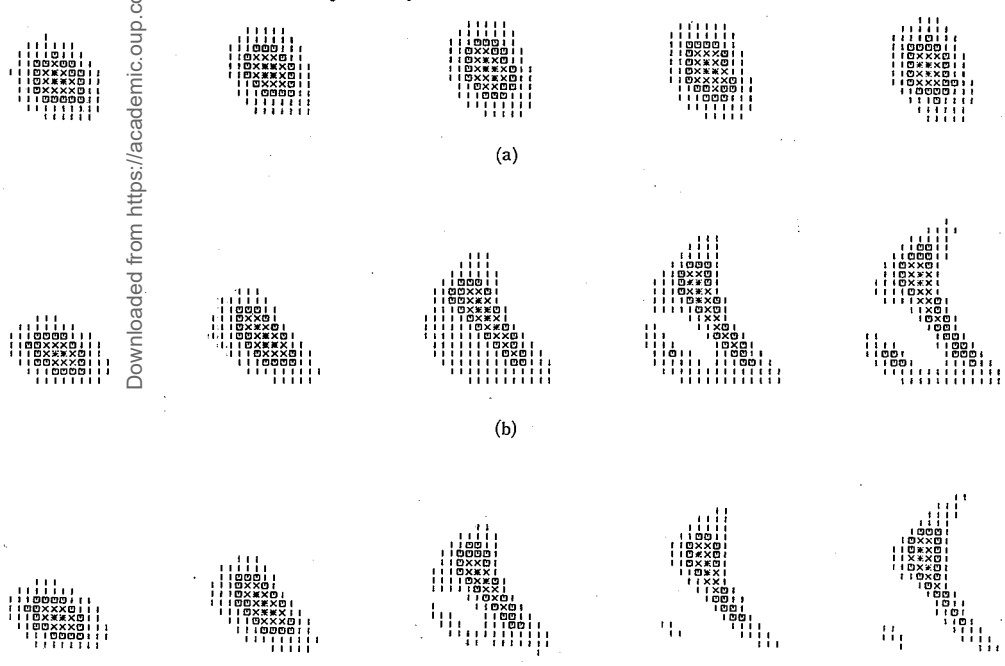

Fig. 6. (continued)

(d)

Fig. 6. Images of the circular objects in (a) $A_{80.1.z}$, (b) $A_{80.2.z}$, (c) $A_{80.3.z}$ and (d) $A_{80.5.z}$ at epochs z=1, 2, 3, 4 and 5 (from left to right).

(a)

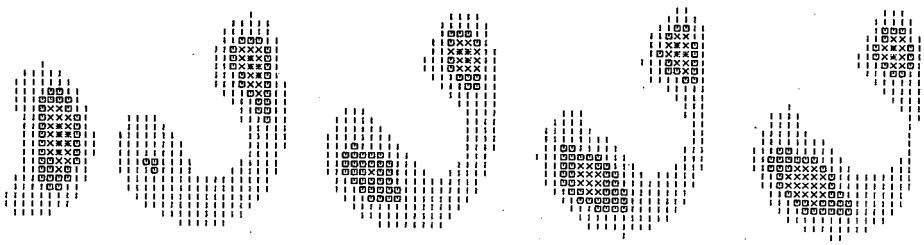

(b)

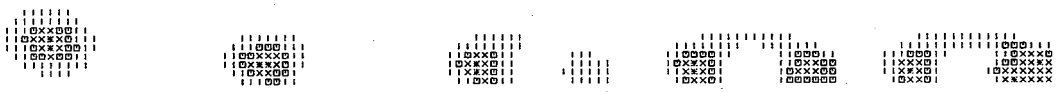

(c)

(d)

Fig. 7. (continued)

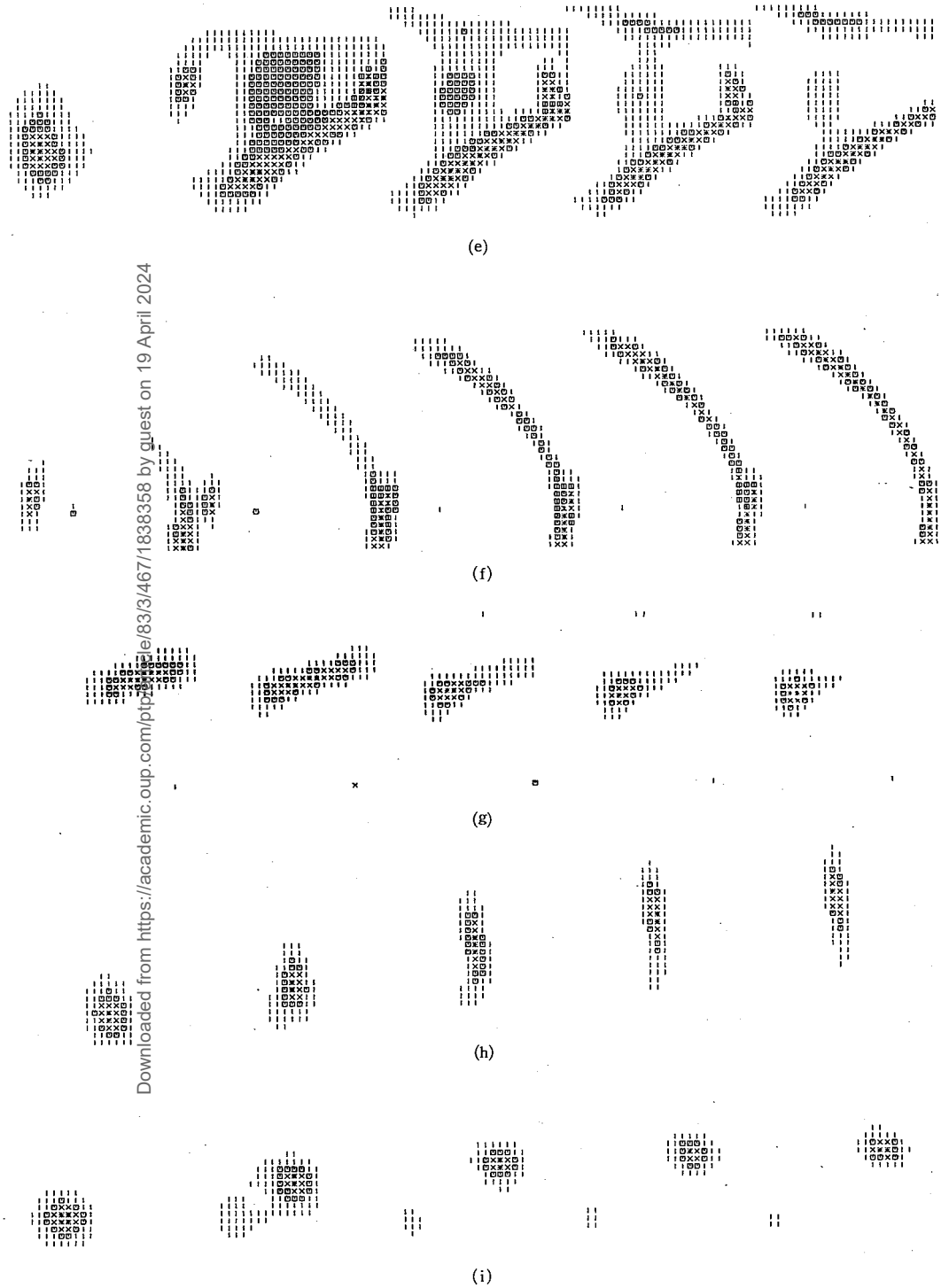

Fig. 7. Images of the circular objects in (a) $B_{80.2.z}$, (b) $C_{80.2.z}$, ⋯, (i) $J_{80.2.z}$ at epochs $z=1$, 2, 3, 4 and 5 (from left to right).

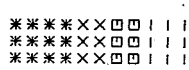

Fig. 8. Linear regions. $*$, $\times$, $\square$, $|$ denote the regions of $14 \leq Y \leq 16$ and $10 \leq X \leq 13$, $13 < X \leq 15$, $15 < X \leq 17$ and $17 < X \leq 20$, respectively.

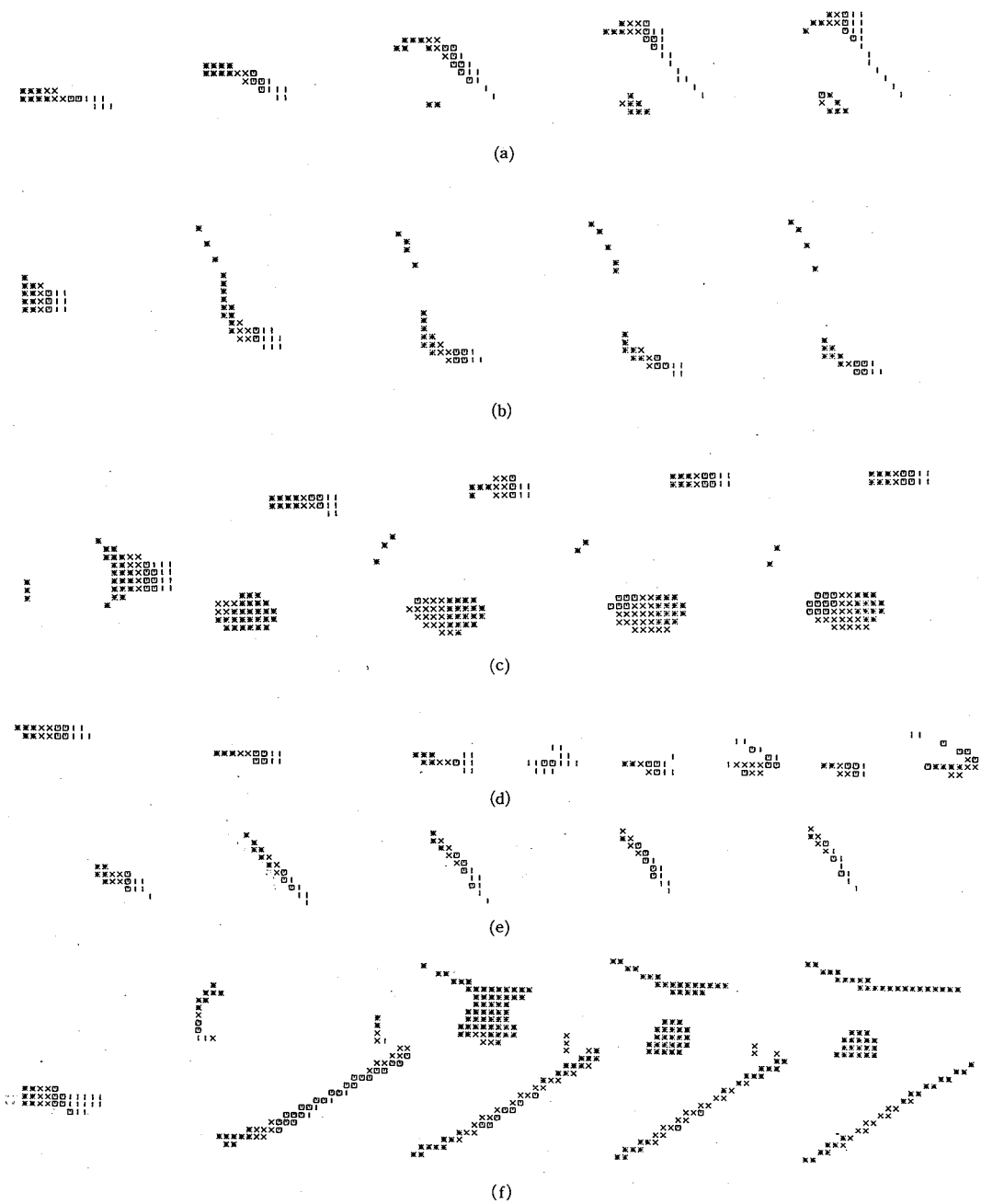

Fig. 9. (continued)

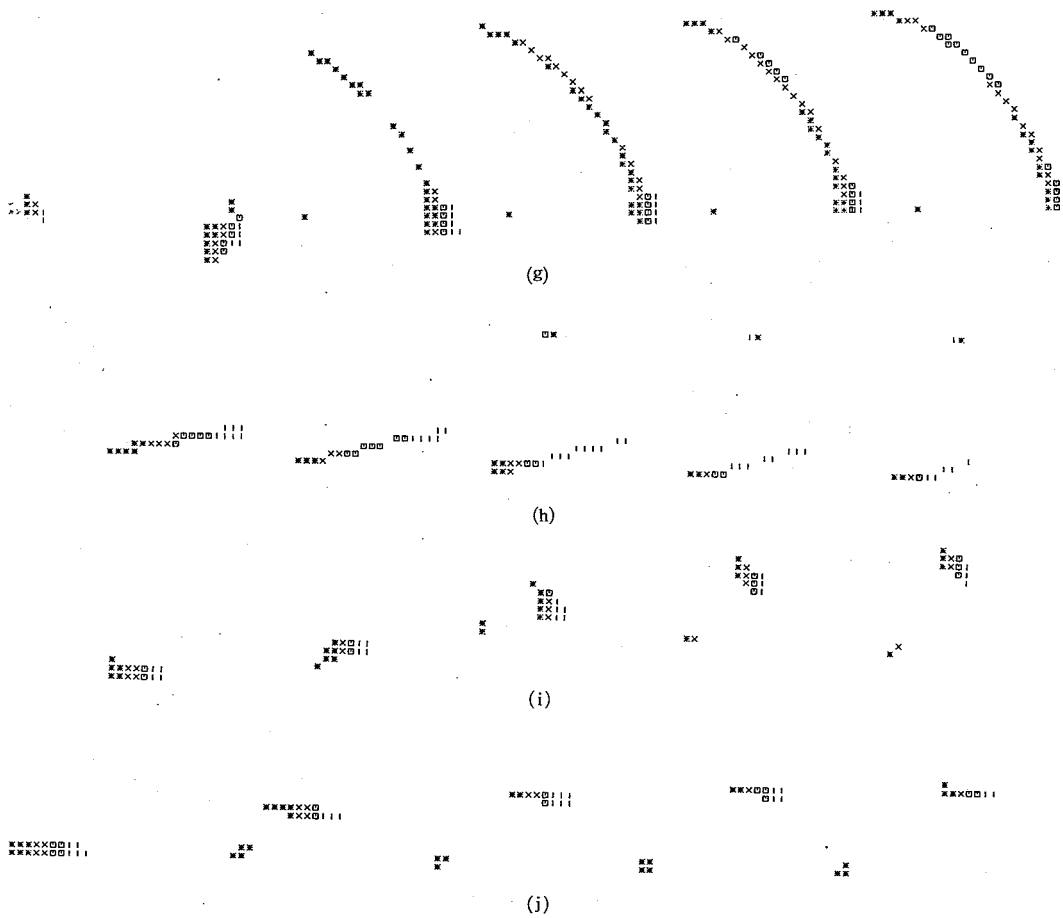

Fig. 9. Images of the linear objects in (a) $A_{80.2.z}$, (b) $B_{80.2.z}$, (c) $C_{80.2.z}$, ⋯, (j) $J_{80.2.z}$ at epochs z=1, 2, 3, 4 and 5 (from left to right).

§ 4. Quantitative analyses of image deformation

In order to represent the characteristic behaviors of image deformation we introduce the following two quantities. One of them is the root of mean squares ($\beta(\theta)$) of the difference of deflection angles of two rays with a separation angle θ divided by θ, which is equal to β and $\sqrt{G}$ in previous works.[5)~7)] It is defined in the present notation as

$$\beta^2(\theta)\equiv\frac{1}{N(\theta)}\sum_{\alpha,\beta}(\delta_\alpha-\delta_\beta)^2\,, \tag{4·1}$$

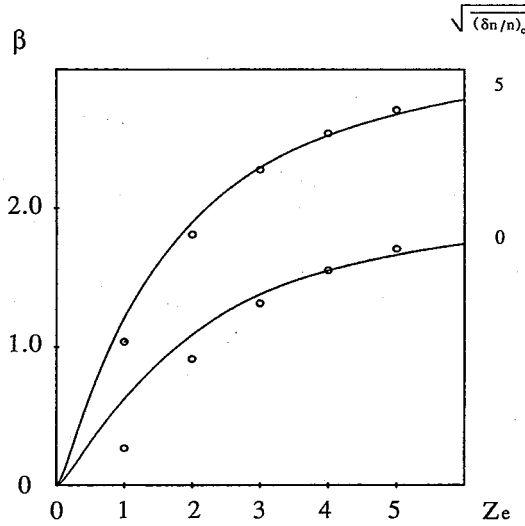

Fig. 10. Mean values of $\beta(0)$ for $l_{\rm eff}=60h^{-1}$kpc and $z_f=2$. Real lines show the values in the simplified model.

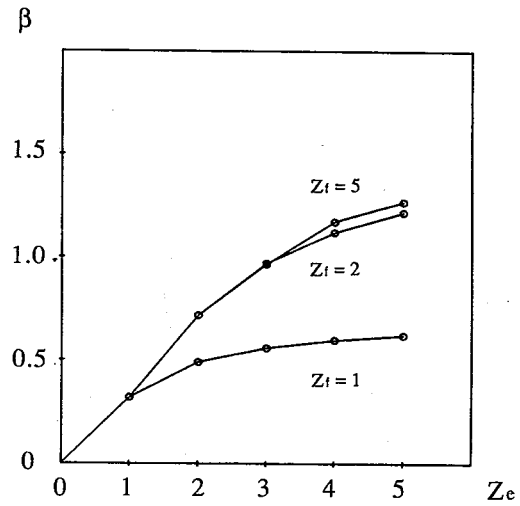

Fig. 12. $\beta(0)$ in $A_{80.1.z}$, $A_{80.2.z}$ and $A_{80.5.z}$ at epochs $z=1-5$.

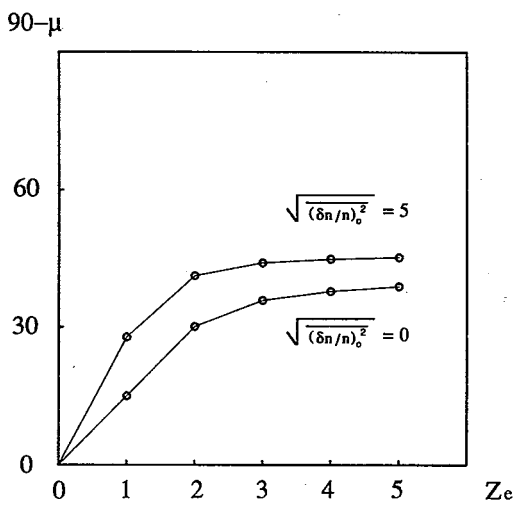

Fig. 11. Mean values of $90-\mu(0)$ (in the degree unit) for $l_{\rm eff}=60h^{-1}$kpc and $z_f=2$.

$$\delta_\alpha\equiv[(\delta y^i e_{(1)i},\ \delta y^i e_{(2)i})/y_B]_\alpha\,, \qquad (4\cdot2)$$

where the indices α and β represent the α and β-th rays with the separation angle $\theta=1, 2, 3, \cdots$ arcsec, and $N(\theta)$ is the number of pairs of rays with the angle θ in a ray bundle. δ_α and hence $\beta(\theta)$ are also functions of z.

Another one is the average angle $\mu(\theta)$ between two vectors $\boldsymbol{r}_\beta-\boldsymbol{r}_\alpha$ and $\boldsymbol{r}_\gamma-\boldsymbol{r}_\alpha$, where $\boldsymbol{r}_\alpha$ is (X_α, Y_α) in the previous section. These two vectors are chosen so as to be perpendicular to each other at the present epoch, that is,

$$(\boldsymbol{r}_\beta-\boldsymbol{r}_\alpha)\cdot(\boldsymbol{r}_\gamma-\boldsymbol{r}_\alpha)=0\,,$$

and satisfy

$$|\boldsymbol{r}_\beta-\boldsymbol{r}_\alpha|=|\boldsymbol{r}_\gamma-\boldsymbol{r}_\alpha|=\theta\,. \qquad (4\cdot3)$$

The quantity μ is defined as

$$\mu(\theta)\equiv\cos^{-1}[cs(\theta)]\,, \qquad (4\cdot4)$$

$$[cs(\theta)]^2\equiv\frac{1}{N'(\theta)}\sum_{\alpha,\beta,\gamma}[(\boldsymbol{r}_\beta-\boldsymbol{r}_\alpha)\cdot(\boldsymbol{r}_\gamma-\boldsymbol{r}_\alpha)]^2/\theta^2\,, \qquad (4\cdot5)$$

where $N'(\theta)$ represents the number of trios of possible rays such that the above conditions (4·3) and (4·4) are satisfied at the present epoch. To express the change in angles we had better use $90-\mu(\theta)$ for $\mu(\theta)$. Here $\mu(\theta)$ is expressed in the degree unit. $cs(\theta)$ and $\mu(\theta)$ are also functions of z.

First we derived ten sets of quantities $\beta(\theta)$ and $90-\mu(\theta)$ at epochs $z=1-5$, which correspond to the ten ray bundles, and next the mean values and the dispersions for the ten sets. They are shown in Tables I, II and III for $l_{\rm eff}=60$, 80 and $120h^{-1}$kpc, respectively. For a comparison these quantities were calculated for another 5 ray bundles also in a case when galaxies were always put only in the grid points and there was no correlation in their positions. Their values are shown in Table IV. It is found that $\beta(\theta)$ and $90-\mu(\theta)$ in the correlated case are larger than those in the non-correlated case, and that also the dispersions in the correlated case are larger. As for $\beta(\theta)$ the values are larger by a factor of about 3. The behaviors $\beta(\theta)$ and $90-\mu(\theta)$ are shown in the cases $l_{\rm eff}=60h^{-1}$kpc in Figs. 10 and 11, respectively. Moreover the mean values of $\beta(0)$ in $A_{80.1.z}$, $A_{80.2.z}$ and $A_{80.5.z}$ are given in Fig. 12, which shows that there is a quantitative difference between their behaviors for $z_f=1$ and those for $z=2-5$.

Table I. Mean values of $\beta(\theta)$ and $90-\mu(\theta)$ and their dispersions $\Delta\beta(\theta)$ and $\Delta\mu(\theta)$ in the case $l_{\rm eff}=60h^{-1}$kpc and $z_f=2$. μ and θ are in units of degree and arcsec, respectively.

z	θ	β	$\Delta\beta$	$90-\mu$	$\Delta\mu$
	1	1.038	0.917	27.844	12.851
	2	1.027	0.933	28.142	13.333
1	3	1.016	0.956	28.396	13.775
	4	0.965	0.865	28.667	13.721
	5	0.895	0.772	28.899	14.662
	1	1.810	1.137	41.194	7.891
	2	1.735	1.123	41.338	7.944
2	3	1.684	1.176	41.171	8.013
	4	1.578	1.043	41.454	8.623
	5	1.444	0.906	40.616	7.602
	1	2.275	1.238	44.041	7.212
	2	2.149	1.183	44.139	6.873
3	3	2.074	1.240	44.065	6.403
	4	1.923	1.090	44.528	7.197
	5	1.768	0.940	44.101	6.575
	1	2.538	1.305	44.877	6.923
	2	2.381	1.223	44.910	6.481
4	3	2.291	1.280	45.048	6.426
	4	2.115	1.118	44.925	7.166
	5	1.949	0.961	45.079	5.165
	1	2.706	1.350	45.260	6.719
	2	2.529	1.251	45.268	6.150
5	3	2.430	1.307	45.362	6.256
	4	2.237	1.136	45.338	7.086
	5	2.065	0.975	45.416	4.912

Table II. Mean values of $\beta(\theta)$ and $90-\mu(\theta)$ and their dispersions $\Delta\beta(\theta)$ and $\Delta\mu(\theta)$ in the case $l_{\rm eff}=80h^{-1}$kpc and $z_f=2$. μ and θ are in units of degree and arcsec, respectively.

z	θ	β	$\Delta\beta$	$90-\mu$	$\Delta\mu$
	1	0.693	0.471	26.795	12.431
	2	0.691	0.482	27.029	12.886
1	3	0.684	0.485	27.494	13.399
	4	0.668	0.458	27.273	13.150
	5	0.657	0.461	27.013	13.852
	1	1.200	0.574	39.945	8.121
	2	1.179	0.578	39.997	8.259
2	3	1.147	0.574	40.420	8.530
	4	1.113	0.538	40.139	8.500
	5	1.080	0.542	39.840	7.045
	1	1.495	0.613	42.713	7.259
	2	1.464	0.612	42.863	6.885
3	3	1.418	0.599	43.023	6.740
	4	1.373	0.568	43.265	7.533
	5	1.328	0.564	43.055	6.530
	1	1.660	0.637	43.655	6.987
	2	1.623	0.632	43.839	6.408
4	3	1.569	0.613	43.816	6.094
	4	1.518	0.585	43.527	6.354
	5	1.466	0.575	43.955	6.240
	1	1.765	0.654	44.042	6.649
	2	1.724	0.646	44.180	6.303
5	3	1.665	0.623	44.310	5.858
	4	1.611	0.596	43.877	6.161
	5	1.555	0.583	43.849	5.530

Table III. Mean values of $\beta(\theta)$ and $90-\mu(\theta)$ and their dispersions $\Delta\beta(\theta)$ and $\Delta\mu(\theta)$ in the case $l_{\rm eff}=120h^{-1}$kpc and $z_f=2$. μ and θ are in units of degree and arcsec, respectively.

z	θ	β	$\Delta\beta$	$90-\mu$	$\Delta\mu$
	1	0.419	0.193	23.069	10.706
	2	0.422	0.200	23.128	11.109
1	3	0.423	0.206	23.247	11.432
	4	0.417	0.198	23.064	11.362
	5	0.421	0.212	22.781	11.837
	1	0.711	0.216	36.788	8.624
	2	0.709	0.225	36.851	8.746
2	3	0.705	0.234	36.758	8.518
	4	0.696	0.223	36.979	9.476
	5	0.691	0.245	35.951	9.008
	1	0.869	0.220	40.317	7.679
	2	0.866	0.228	40.605	7.536
3	3	0.860	0.237	40.972	7.291
	4	0.848	0.227	40.477	7.836
	5	0.840	0.251	40.185	6.422
	1	0.958	0.223	41.606	7.440
	2	0.954	0.232	41.607	7.385
4	3	0.947	0.241	41.638	6.822
	4	0.933	0.230	41.708	7.534
	5	0.924	0.254	41.231	6.603
	1	1.014	0.227	42.314	7.247
	2	1.010	0.235	42.467	6.985
5	3	1.003	0.244	42.555	6.603
	4	0.987	0.233	42.766	7.138
	5	0.978	0.257	42.472	6.657

Table IV. Mean values of $\beta(\theta)$ and $90-\mu(\theta)$ and their dispersions $\Delta\beta(\theta)$ and $\Delta\mu(\theta)$ in the case $l_{\rm eff}=60h^{-1}$kpc and $z_f=2$, when galaxies are always put at the grid points. μ and θ are in units of degree and arcsec, respectively.

z	θ	β	$\Delta\beta$	$90-\mu$	$\Delta\mu$
	1	0.269	0.111	15.092	6.891
	2	0.252	0.090	14.311	6.046
1	3	0.235	0.072	13.818	5.472
	4	0.242	0.080	14.029	5.722
	5	0.201	0.031	12.494	4.066
	1	0.912	0.384	30.126	6.296
	2	0.808	0.244	29.683	5.958
2	3	0.697	0.152	29.145	5.693
	4	0.689	0.137	28.944	5.234
	5	0.542	0.098	28.282	7.173
	1	1.312	0.479	35.830	5.807
	2	1.170	0.306	35.482	5.636
3	3	1.021	0.221	34.589	5.535
	4	0.988	0.182	34.427	4.875
	5	0.795	0.176	32.046	7.609
	1	1.552	0.551	37.800	5.413
	2	1.381	0.349	37.222	5.064
4	3	1.211	0.260	37.029	5.570
	4	1.163	0.213	36.837	4.622
	5	0.943	0.212	34.339	5.717
	1	1.707	0.600	38.859	5.056
	2	1.518	0.378	38.143	4.532
5	3	1.333	0.284	38.126	5.102
	4	1.276	0.233	38.078	4.432
	5	1.038	0.232	34.900	5.772

§ 5. A simplified model of multiple deflections

In this section metric perturbations are considered in the form of gravitational deflection angles due to the nearest individual galaxies and comparatively small gravitational forces from surrounding galaxies are neglected for simplicity. Moreover it is assumed that the distribution of galaxies are approximately uniform, in such a way that their spatial correlation length is about $5h^{-1}$Mpc at present. Then the average deflection angle is derived as follows: First let us denote the average coordinate distance between two nearest galaxies as r_b and the average number density of galaxies as $n(=1/(r_b a)^3)$, and consider the deflections by galaxies in the time interval $t_0 \geq t \geq t_f$. Because the individual deflections and the deviation of galactic number density from the mean value are random, the mean deflection angle is given by

$$\overline{(\delta\theta)^2}=\int_0^{\mathrm{Min}(\lambda_e,\lambda_f)}d\lambda\int_0^{r_b}dr\,2\pi r(na^3)\left[1+\overline{\left(\frac{\delta n}{n}\right)^2}\right]\left(\frac{4Gm}{ac^2}f(r)\right)^2\Phi^2(t)\,, \tag{5·1}$$

where λ is the coordinate length from the observer to a lens object at epoch t given by

$$a_0\lambda=a_0\int_t^{t_0}cdt/a=(2c/H_0)[1-(1+z)^{-1/2}]\,, \tag{5·2}$$

$a_0\equiv a(t_0)$, and Φ is a factor transforming the angle at epoch t to the angle at the present epoch t_0 and expressed as

$$\Phi(t)\equiv(\lambda_e-\lambda)/\lambda_e=[(1+z)^{-1/2}-(1+z_e)^{-1/2}]/[1-(1+z_e)^{-1/2}] \tag{5·3}$$

with $\lambda_e\equiv\lambda(t=t_e)$. t_e is the emission time. Moreover m is the total galactic mass and $\{4Gm/(ac^2)\}f(r)\boldsymbol{r}/r$ is the deflection angle vector around a galaxy with the mass distribution $m(r/R)$ which is given in Eq. (A·8). Its functional form is derived using the formula of deflection angles for an extended lens[8] and expressed as

$$f(r)=\frac{r}{r^2+(R\epsilon)^2}\,. \tag{5·4}$$

Since the coordinate length between two rays with the separation angle θ is $\theta\lambda$, on the other hand, the relative deflection angle-angle ratio β is given by

$$\beta^2\theta^2=\int_0^{\mathrm{Min}(\lambda_e,\lambda_f)}d\lambda(na^3)\left[1+\overline{\left(\frac{\delta n}{n}\right)^2}\right]\Phi^2(t)$$
$$\times\int_0^{r_b}2\pi rdr\int_0^{2\pi}\frac{d\phi}{2\pi}\left(\frac{4Gm}{c^2a}\left[\frac{f(r)}{r}\boldsymbol{r}-\frac{f(r')}{r'}\boldsymbol{r}'\right]\right)^2\,, \tag{5·5}$$

where the position vectors of the two rays in the perpendicular plane are $\boldsymbol{r}$ and $\boldsymbol{r}'$ and the angle between the vectors $\boldsymbol{r}$ and $\boldsymbol{r}-\boldsymbol{r}'(=\lambda\boldsymbol{\theta})$ is ϕ (cf. Fig. 14). Then we get the following relations among $\boldsymbol{r}$, $\boldsymbol{r}'$ and ϕ:

$$r'^2=r^2+(\lambda\theta)^2-2r(\lambda\theta)\cos\phi\,, \tag{5·6}$$

$$\boldsymbol{r}\boldsymbol{r}'/(rr')=(r-\lambda\theta\cos\phi)/r'\,. \tag{5·7}$$

Equation (5·5) can be rewritten as

$$\beta^2=8\pi\left(\frac{4Gm}{c^2aR\epsilon}\right)^2n_0(c/H_0)^3(I_1+I_2)\,, \tag{5·8}$$

$$I_1\equiv[1-(1+z_e)^{-1/2}]^{-2}\int_0^{\mathrm{Min}(z_e,z_f)}dz(1+z)^{-3/2}$$
$$\times[1-(1+z)^{-1/2}]^2[(1+z)^{-1/2}-(1+z_e)^{-1/2}]^2J\,, \tag{5·9}$$

$$I_2\equiv[1-(1+z_e)^{-1/2}]^{-2}\int_0^{\mathrm{Min}(z_e,z_f)}dz(1+z)^{-3/2}$$
$$\times[1-(1+z)^{-1/2}]^2[(1+z)^{-1/2}-(1+z_e)^{-1/2}]^2\overline{(\delta n/n)^2}J\,, \tag{5·10}$$

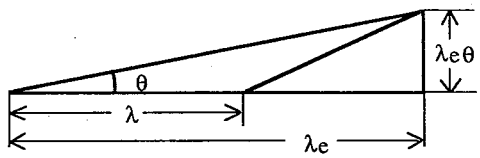

Fig. 13. Transformation of angles.

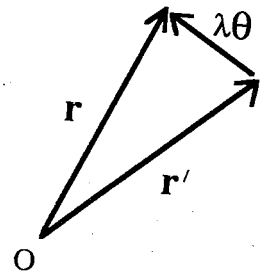

Fig. 14. Vectors in the perpendicular plane.

$$J\equiv\gamma^{-2}\int_0^{r_b/(R\epsilon)}dpp\left(\frac{p^2}{(p^2+1)^2}+\int_0^{2\pi}\frac{d\phi}{2\pi}\left[\frac{p'^2}{(p'^2+1)^2}-\frac{2p^2\left(1-\frac{\gamma}{p}\cos\phi\right)}{(p^2+1)(p'^2+1)}\right]\right), \quad (5\cdot11)$$

where $\gamma\equiv\theta\lambda/(R\epsilon)$, $p\equiv r/(R\epsilon)$ and $p'^2=p^2+\gamma^2-2\gamma p\cos\phi$.

The integration of J is complicated, but nearly independent of r_b, because of $r_b\gg\theta\lambda$ in the present case. By numerical calculations we find that, for $z\gtrsim2$, J is nearly equal to 0.4 and roughly independent also of z. In a separate paper the accurate treatment of this integral will be performed and the behaviors of β and μ will be shown. Here β is estimated assuming that J is 0.4.

If J is constant, the integrals, I_1 and I_2 are performed as follows: For I_1 we obtain in the case $z_e\leq z_f$

$$I_1=\frac{1}{15}u_e^3J \quad (5\cdot12)$$

and in the case $z_e>z_f$

$$I_1=\frac{1}{15}u_f^3u_e^{-2}(6u_f^2-15u_fu_e+10u_e^2)J\,, \quad (5\cdot13)$$

where $u_e\equiv1-(1+z_e)^{-1/2}$ and $u_f\equiv1-(1+z_f)^{-1/2}$. For I_2 we must specify the time dependence of $\overline{(\delta n/n)^2}$. Here for simplicity we assume that $\overline{(\delta n/n)^2}=\overline{(\delta n/n)_0^2}(1+z)^{-2}$, as if always in the linear stage. Since $\overline{(\delta n/n)_0^2}\sim1$ in the scale of $5h^{-1}$Mpc, we get $\overline{(\delta n/n)_0^2}\sim5$ in the scale r of the unit box per a galaxy ($=3h^{-1}$Mpc), if we assume the Poisson law $\sqrt{\overline{(\delta n/n)^2}}\propto(nr^3)^{-1/2}$. Then in the case $z_e\leq z_f$

$$I_2=\frac{1}{15}u_e^3\left[1-2u_e+\frac{12}{7}u_e^2-\frac{5}{7}u_e^3+\frac{5}{42}u_e^4\right]J\overline{(\delta n/n)_0^2} \quad (5\cdot14)$$

and in the case $z_e>z_f$

$$I_2=\frac{1}{15}u_f^3u_e^{-2}\left[\frac{10}{3}u_f^6-\frac{15}{2}(u_e+2)u_f^5+\frac{30}{7}(u_e^2+8u_e+6)u_f^4-20(u_e^2+3u_e+1)u_f^3\right.$$
$$\left.+6(6u_e^2+8u_e+1)u_f^2-15u_e(2u_e+1)u_f+10u_e^2\right]J\overline{(\delta n/n)_0^2}\,. \quad (5\cdot15)$$

Moreover the coefficient of Eq. (5·5) is

$$\beta_0^2 \equiv \beta^2/(I_1+I_2)$$
$$=580\left(\frac{m}{7.9\times10^{12}h^{-1}M_\odot}\right)\left(\frac{10h^{-1}\mathrm{kpc}}{aR\epsilon}\right)^2, \qquad (5\cdot16)$$

where we used $n_0=\rho_0/m$ and $8\pi G\rho_0=3H_0^2$. In Fig. 10 the behaviors of β^2 in the case $6R\epsilon=60h^{-1}$kpc, $J=0.4$ and $z_f=2$ are shown together with the values of β^2 derived in the previous section. Here we consider the case $\overline{(\delta n/n)_0^2}=5$ and 0. The latter case corresponds to the case when galaxies are put only to grid points. It is found that the values of β^2 in this simplified model are consistent with those in our simulation shown in the previous section, though some deviations can be seen at $z\lesssim1$. These deviations come from that the approximate relation $J=$constant is not good at $z\lesssim1$. The similar situation is found in deflection angle $\overline{(\delta\theta)^2}$.

For given $z_f(=1, 2$ and $5)$, the relations between β and z_e are shown in Fig. 15. It is found from this figure that the relations with $z_f\geq2$ are similar to each other, but different from those with $z_f=1$. A similar situation was found in the result of the numerical calculations in §§ 3 and 4. This situation is explained as follows: Galaxies at earlier epochs arouse more deflections, because their number density n is larger. On the other hand, as lenses are nearer to the emitters, the deflection angles measured by the observer (at epoch t_0) are smaller. This effect is represented by Φ^2 for the equations for β. Because of the above two effects, the main contribution to the integrals I_1 and I_2 comes from the redshift interval $z=0.3-1.0$ and $0.3-1.5$ for $z_f=1$ and $z_f\geq2$, respectively. Accordingly, the integrated behaviors are different in the case $z_f=1$ and the case $z_f\geq2$.

Moreover it is interesting to notice the dependence of β on m. Because $n_0\propto m^{-1}$, the radius$\simeq6aR\epsilon$ and observationally $m/($the radius$)\propto m^\alpha$ $(\alpha=0.3-0.4)$,[9] we obtain

$$\beta_0\propto m^{-(0.5-\alpha)}. \qquad (5\cdot17)$$

This means that β is larger for smaller m, if the mass density of lenses is constant. For instance, put $\alpha=0.35$. Then β and G are by factors 1.4 and 2.0 larger, re-

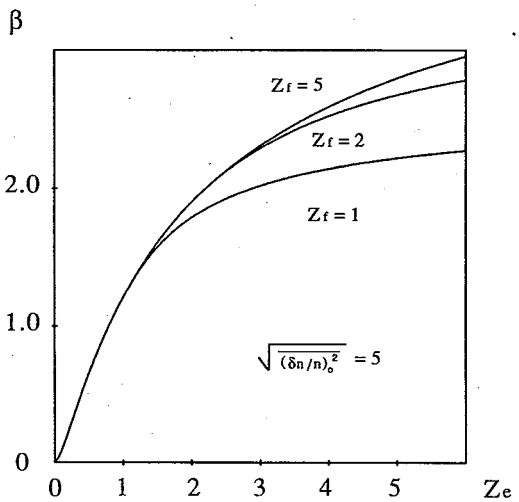

Fig. 15. Dependence of β on z_f for $0\leq z_e\leq5$.

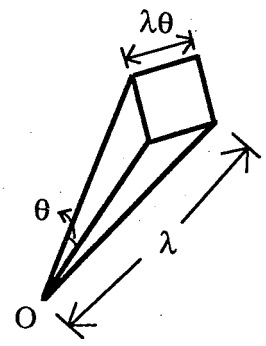

Fig. 16. A light cone.

spectively, as m is by a factor 10 smaller. Though we assumed the comparatively larger mass for galaxies, therefore, the image deformation will be larger, when we assume smaller masses. As for the θ dependence, on the other hand, the lens effect in this case will arise in smaller angles.

Next let us consider how many galaxies are included within the angular area θ^2. The number of galaxies in a cone, whose cross section is a square such as in Fig. 16, is

$$\theta^2 n_0 (a_0 \lambda_e)^3/3 . \tag{5·18}$$

Accordingly the number of galaxies is given by

$$N(z_e)=55(\theta/30)^2[1-(1+z_e)^{-1/2}]^3 , \tag{5·19}$$

where θ is in the arcsec unit. For $z_e=1$, 2, 3 and 5, we get respectively

$$N=(1.4,\ 4.2,\ 6.9 \text{ and } 11)(\theta/30)^2 . \tag{5·20}$$

§ 6. Concluding remarks

We have studied the gravitational lens effect due to galaxies on the images of high redshift objects and found that the deformation is so large to explain the observed warping of high redshift quasars. Quantitative analyses of the deformation and the explanation of their results in a simplified model also have been performed. As a result we have found that β depends sensitively on the particle size but the dependence of μ on the size is smaller, and that the contribution of $\overline{(\delta n/n)_0^2}$ to β is significant.

On the other hand there are some problems in our inhomogeneous models. First we assumed that all matter in the universe consists of galaxies with the same mass and the existence of uncondensed matter was neglected. If the latter matter is dominant, our results must be modified, so that the lens effect is weaker. Second, because the size of the periodic box is $33.3h^{-1}$Mpc, larger inhomogeneities such as groups of clusters and superclusters could not be taken into account.

If we consider microlensing due to lens objects with smaller mass m, β and the image deformation will be larger in smaller scales. The deformation for $z \gtrsim 5$ may therefore be large enough for small objects with a few arcsec to be discriminated observationally. This situation may explain also why quasars with $z \gtrsim 5$ cannot easily be found.

Moreover it is important in our work to clarify the mass and radius of the halo component of galaxies. These problems will be examined in future works.

Acknowledgements

The present work is supported in part by the Japanese Grant in Aid for Science Research Fund of the Ministry of Education, Science and Culture No. 61540185. One of the authors (K.T.) thanks Professor K. Aizu for helpful discussions about high redshift quasars. Numerical calculations were performed using the supercomputer

FACOM VP4 in the Computer Center of Kyoto University.

Appendix

—— Numerical Methods ——

Inhomogeneous models were derived using the same method as in the previous paper,[5] that is, our code was made on the basis of Aarseth's individual time step method, except for that the size of the periodic box was contracted by a factor 6. The calculated positions of particles were kept in a file and next used for the calculations of light paths. For the latter calculations the Adams integration method was used.

The Poisson equation is replaced by

$$\frac{\partial^2\phi}{\partial \boldsymbol{y}^2}=\frac{8\pi G}{c^2 a}(aR)^2[\rho(\boldsymbol{y})-\rho_B]=4\pi e^{-2\tau}[\rho(\boldsymbol{y})/\rho_B-1]\,. \tag{A·1}$$

Here the inhomogeneity is inside a periodic box such that the relevant point is the center and the region outside the box is assumed to be homogeneous. In the box there are N particles. If $\rho(\boldsymbol{y})$ is given by delta functions as

$$\rho(\boldsymbol{y})=m\sum_{\alpha=1}^{N}\delta(aR(\boldsymbol{y}-\boldsymbol{y}_\alpha))\,, \tag{A·2}$$

we obtain

$$\begin{aligned}&\phi=\phi_1+\phi_2\,,\\ &\phi_1=-e^{-2\tau}\sum_{\alpha=1}^{N}\frac{1}{|\boldsymbol{y}-\boldsymbol{y}_\alpha|}\,,\\ &\phi_2=e^{-2\tau}\int d\boldsymbol{y}'/|\boldsymbol{y}-\boldsymbol{y}'|\,.\end{aligned} \tag{A·3}$$

The latter potential ϕ_2 comes from the homogeneous background density, so that its gradient gives no force to particles. Now in order to take into account the finite particle size, we modify the expression of ϕ_1 in Eq. (A·3) as

$$\phi_1=-e^{-2\tau}\sum_{\alpha=1}^{N}[|\boldsymbol{y}-\boldsymbol{y}_\alpha|^2+\epsilon^2(\tau)]^{-1/2}\,, \tag{A·4}$$

where the softening parameter $\epsilon(\tau)$ gives the size of the core of the particles in comoving coordinates. Since for $0\leq z\leq 5$ the physical size of galaxies is constant in the present treatment, we have

$$\epsilon(\tau_0)=\epsilon_5/6\,, \tag{A·5}$$

where ϵ_5 is ϵ at the epoch $z=5$. The mass density distribution corresponding to the potential (A·2) is given by

$$\rho(\boldsymbol{y})=m\sum_{\alpha=1}^{N}f(\boldsymbol{y}-\boldsymbol{y}_\alpha) \tag{A·6}$$

with

$$f(\boldsymbol{y}-\boldsymbol{y}_a)=\frac{3}{4\pi}\frac{\epsilon^2}{(aR)^3}[|\boldsymbol{y}-\boldsymbol{y}_a|^2+\epsilon^2]^{-5/2}. \tag{A·7}$$

The mass distribution for each particle, therefore, is defined by

$$\frac{m(y)}{m}\equiv(aR)^3\int_0^y f(\boldsymbol{y})d^3\boldsymbol{y}=3\int_0^{y/\epsilon} duu^2/(u^2+1)^{5/2}=[w^3/(w^2+1)^{3/2}]_{w=y/\epsilon}, \tag{A·8}$$

where $m(y)$ is the mass within a sphere of the radius y. For $y=\epsilon$, $m(y)/m=0.35$ and, for $y=(3 \text{ and } 6)\epsilon$, $m(y)/m=0.86$ and 0.97, respectively. Hence $l_{\text{eff}}(\equiv 6a_0R\epsilon)$ can be regarded as the effective radius of a particle. We assume that the present radius of galaxies, $6Ra_0\epsilon(\tau_0)$, is $(60, 80 \text{ or } 120)h^{-1}$kpc, so that we get ϵ_5 is 0.02, 0.0267 or 0.04, respectively, because $a_0R=(33.3/11)h^{-1}$Mpc.

References

1) P. D. Bartel and G. K. Miley, Nature **333** (1988), 319.
2) P. D. Bartel, G. K. Miley, R. T. Schilizzi and C. J. Lonsdale, Astron. Astrophys. Suppl. **73** (1988), 515.
3) R. D. Blandford and M. Jaroszynski, Astrophys. J. **246** (1981), 1.
4) K. Miyoshi and T. Kihara, Publ. Astron. Soc. Jpn. **27** (1975), 333.
5) K. Tomita and K. Watanabe, Prog. Theor. Phys. **82** (1989), 512.
6) K. Tomita, Phys. Rev. **D40** (1989), 111.
7) M. Sasaki, Month. Not. Roy. Astron. Soc. **240** (1989), 415.
8) R. R. Bourassa and R. Kantowski, Astrophys. J. **195** (1975), 13.
9) H. J. Rood, Rep. Prog. Phys. **44** (1981), 1081.